Available online at www.sciencedirect.com
ScienceDirect
International Journal of Mass Spectrometry 265 (2007) 124–129
International Journal of Mass Spectrometry
www.elsevier.com/locate/ijms

Effect of the surface morphology on the energy transfer in ion–surface collisions☆

Zhibo Yang, Omar Hadjar, Julia Laskin *

Pacific Northwest National Laboratory, Fundamental Science Directorate, P.O. Box 999, K8-88 Richland, WA 99352, USA

Received 2 November 2006; received in revised form 24 January 2007; accepted 25 January 2007
Available online 3 February 2007

Abstract

Time- and energy-resolved surface-induced dissociation (SID) of singly protonated des-Arg[1]-bradykinin (PPGFSPFR) combined with RRKM modeling was used to explore the effect of surface morphology on the energy transfer in collisions of large ions with surfaces. Experiments were performed in a Fourier Transform ion cyclotron resonance mass spectrometer (FT-ICR MS) specially configured for SID studies. Mass-selected and vibrationally relaxed ions were collided with three diamond surfaces of varying degree of roughness along the surface normal. The results demonstrate that internal energy distributions resulting from collisions of large ions with surfaces are rather independent of the surface morphology: the translational to vibrational (T → V) energy transfer efficiency is 19.5 ± 0.5% for all three diamond surfaces. However, the scattered ion signal increases by a factor of 2 with decrease in the degree of roughness of the SID target suggesting that smooth diamond surfaces are better targets for analytical applications.
Published by Elsevier B.V.

Keywords: Surface-induced dissociation; Protonated peptide; Energy transfer; Surface morphology; FT-ICR MS

1. Introduction

Excitation of ions by collisions with surfaces is a powerful method for the activation and dissociation of large ions in a mass spectrometer [1–3]. During ion–surface collision part of ion's kinetic energy is converted into its internal energy resulting in surface-induced dissociation (SID) of the vibrationally excited species. The efficiency of translational to vibrational (T → V) energy transfer for collisions of large peptide ions with surfaces shows only minor dependence on the collision energy and the identity of the ion [4–11] and is largely determined by the physical properties of the surface.

Organic thin films on metal substrates are commonly used as SID targets. These include homogeneous self-assembled monolayers (SAMs) on gold or silver [1,12], mixed fluorocarbon/hydrocarbon (FSAM/HSAM) on gold surface [13], Langmuir–Blodgett (L–B) films [14], thin films of a liquid perfluoropolyether (PFPE) [15,16] or residual pump oil on stainless steel [17–21]. The percent of T → V transfer is in the range of 17–28% for fluorinated SAM surfaces (FSAM) [8,22,23], PFPE [15] and fluorinated L–B films [14]. Lower values of T → V transfer efficiency of 10–15% were reported for SAMs of alkyl thiols on gold (HSAM) [1,3–5,12] and stearate L–B films [14]. Consistent with these observations, the T → V transfer efficiency increases with increase in proportion of the FSAM in the mixed FSAM/HSAM layers [13]. Inorganic surfaces, such as Au{1 1 1} [24], highly oriented pyrolytic graphite (HOPG) [25], thin films of LiF [8] and carbon vapor deposited (CVD) diamond [8] have been also utilized for SID of polyatomic projectiles. T → V transfer efficiencies reported for these SID targets are 15% for HOPG [25], 30% for clean Au surface [24], 12% for LiF [8], 17–24% for diamond [4,8–10].

It has been suggested that the effective mass of the surface determines the T → V transfer efficiency [23,26–28]. Several groups demonstrated that only the end groups of organic molecules composing the thin film are responsible for ion excitation [14,16,29,30] and the difference in energy transfer on fluorinated and hydrocarbon surfaces reflects differences in effective masses of target species. Classical trajectory simula-

☆ It is a great pleasure for us to honor scientific achievements of Jean Futrell—our mentor and friend.

* Corresponding author at: Chemical & Materials Sciences Division, Pacific Northwest National Laboratory, P.O. Box 999, K8-88 Richland, WA 99352, USA. Tel.: +1 509 376 4443; fax: +1 509 376 6066.
E-mail address: Julia.Laskin@pnl.gov (J. Laskin).

1387-3806/$ – see front matter. Published by Elsevier B.V.
doi:10.1016/j.ijms.2007.01.018

tions by Hase and co-workers [4,5,31] suggested that surface stiffness plays a major role in the energy transfer process. Collisions of ions with soft surfaces are characterized by deeper penetration of the ion into the surface resulting in longer interaction times and efficient transfer of a large fraction of the initial kinetic energy of the ion into surface vibrations [4]. In contrast, more efficient partitioning of energy into vibrational excitation of the projectile ion occurs during collisions with a stiffer diamond surface.

Our SID studies of collisions of the singly protonated des-Arg^1-bradykinin with different surfaces [8] demonstrated that collisions of peptide ions with stiff crystalline surfaces result in deposition of wider distributions of internal energies than collisions with soft SAM surfaces. We suggested that surface stiffness has a major effect on the width of the energy deposition function (EDF), while the average energy deposited into the ion is mainly affected by the mass of the chemical moiety constituting the collision partner for the ion impacting the surface. We have also demonstrated that high T → V transfer efficiency and broad EDF deposited into peptide ions by collisions with diamond surface result in significantly improved peptide ion sequence coverage [32,33]. It follows that diamond surface is a superior target for practical applications of SID for peptide and protein identification [32].

Surface morphology is another important factor that may have an effect on the T → V transfer efficiency [34]. Understanding the effect of surface roughness on the energy transfer is important both for practical applications and for comparison of the experimental data with the results of classical trajectory calculations that utilize atomically flat targets. Here we present a first quantitative investigation of the effect of surface morphology on the energy transfer in collisions of peptide ions with diamond surfaces using time- and energy-resolved SID experiments [11]. The T → V transfer efficiency and the EDF are determined using singly protonated des-Arg^1-bradykinin (PPGFSPFR) as a "thermometer ion". The energetics and dynamics of unimolecular dissociation of des-Arg^1-bradykinin have been reported [35] and utilized in our previous study on the energy transfer in collisions of peptide ions with different surfaces [8]. The internal energy distributions of excited ions are derived from RRKM modeling of time- and energy-resolved SID data.

2. Experimental

2.1. Mass spectrometry

SID experiments were conducted using a specially fabricated 6T FT-ICR mass spectrometer described in detail elsewhere [36]. The instrument is equipped with an external electrospray ionization source consisting of an ion funnel [37] followed by three quadrupoles. Ions exiting the ion funnel undergo collisional relaxation and focusing in the first collisional quadrupole prior to transfer into a mass-resolving quadrupole. Mass-selected ions are efficiently thermalized in the accumulation quadrupole, which allows us to remove any internal and translational energy originating from the ion source and ion funnel. After accumulation, ions are extracted from the third quadrupole and transferred into the ICR cell where they collide with the surface along the surface normal. Scattered ions are captured by raising the potentials on the front and rear trapping plates of the ICR cell by 10–20 V. Immediately following the reaction delay, ions are excited by a broadband chirp and detected. The collision energy is defined by the difference in the potential applied to the accumulation quadrupole and the potential applied to the rear trapping plate and the SID target. The ICR cell can be offset above or below ground by as much as ±150 V. Lowering the ICR cell below ground while keeping the potential on the third quadrupole fixed increases collision energy for positive ions. Data acquisition was accomplished with a MIDAS data station developed by Marshall and co-workers at the National High Magnetic Field Laboratory [38].

Time-resolved spectra were obtained by varying the delay between the gated trapping and the excitation/detection event (the reaction delay). Typical experiment involved changing the collision energy across a relatively wide range from 11 to 65 eV in 2 eV increments for six reaction delay times of 1 ms, 5 ms, 10 ms, 50 ms, 0.1 s, and 1 s. Time-dependent survival curves (SCs) were constructed from experimental mass spectra by plotting the relative abundance of the precursor ion as a function of collision energy for each reaction delay.

Three diamond surfaces were investigated in this study. Surface A is a polished chemical vapor deposited (CVD) diamond layer on a silicon wafer; surface B is a CVD layer of diamond on a titanium substrate; surface C is a rough (not polished) CVD diamond layer on a silicon wafer. Surfaces A and C were purchased from Applied Diamond Inc. (Wilmington, DE), and surface B was purchased from P1 Diamond Inc. (Santa Clara, CA). All the surfaces were ultrasonically cleaned in ethanol for 20 min to remove contamination prior to AFM and SID experiments.

Des-Arg^1-bradykinin was purchased from Sigma–Aldrich (St. Louis, MO). The sample was dissolved in 50:50 (v/v) methanol:water solution with 1% acetic acid to a final concentration of about 50 μM. A syringe pump (Cole Parner, Vernon Hills, IL) was used for direct infusion of the electrospray sample at a flow rate of about 25 μl/h.

2.2. Atomic force microscopy (AFM)

Surface morphology was characterized using atomic force microscopy (AFM). All AFM measurements were performed by using a Digital Instruments^{TM} Nanoscope IIIa MultiMode scanning probe microscope (Veeco Metrology Group, Santa Barbara, CA). Tapping-mode AFM images were collected in air, using ultra-sharp (radius of curvature <10 nm, cone side angle ∼17°) silicon nanoprobes (Veeco Metrology Group, Santa Barbara, CA). The cantilevers were ∼125 μm long and 30 μm wide with no coating. The spring constant is about 40 N/m and the resonance frequency is in the range of 338–376 kHz.

2.3. RRKM modeling

The SCs were modeled using an RRKM-based approach developed by our group [39,40]. Energy-dependent microcanon-

ical rate constants for the total decomposition of the precursor ion, $k(E)$, were calculated using the RRKM/QET expression:

$$k(E) = \frac{\sigma W^{\ddagger}(E - E_0)}{h\rho(E)} \quad (1)$$

where $\rho(E)$ is the density states of the reactant, $W^{\ddagger}(E - E_0)$ is the sum of states of the transition state, E_0 is the threshold energy, h is the Planck's constant, and σ is the reaction path degeneracy.

Relative abundance of the precursor as a function of the internal energy and the experimental observation time (t_r), $F(E, t_r)$, was calculated taking into account radiative cooling of the vibrationally excited ion. The energy deposition function (EDF) was described by the following analytical expression [39,40]:

$$P(E, E_{coll}) = \frac{1}{C}(E - \Delta)^l \exp\left(-\frac{E - \Delta}{f(E_{coll})}\right) \quad (2)$$

where $C = \Gamma(l + 1)[f(E_{coll})]^{l+1}$ is a normalization factor, l and D are parameters, and $f(E_{coll})$ has the form:

$$f(E_{coll}) = A_2 E_{coll}^2 + A_1 E_{coll} + A_0 \quad (3)$$

where A_0, A_1, and A_2 are parameters, and E_{coll} is the collision energy.

Finally, the normalized abundance of the precursor ions for each collision energy, E_{coll}, and reaction time, t_r, was calculated using the following expression:

$$I(E_{coll}) = \int_0^{\infty} F(E, t_r) P(E, E_{coll})\, dE \quad (4)$$

The dissociation model for des-Arg^1-bradykinin was adopted from our previous study [35]. The decay of the precursor ion was modeled using two rate constants corresponding to the slow (statistical) decay and fast dissociation by shattering. The shattering component is modeled assuming that the ion fragments instantaneously after reaching the shattering threshold energy. The breakdown curve was kept the same for experiments on different surfaces, while the EDF was varied to yield the best fit between the calculated and experimental parent ion survival curves.

3. Results and discussion

3.1. Morphology of diamond surfaces

Fig. 1 shows the AFM images (left) along with typical section analyses (right) of the three SID diamond targets of varying degree of roughness utilized in this work. The roughness of the surface, quantitatively characterized by the substrate depth, is 3 nm for surface A, 33 nm for surface B, and 1.1 μm for surface C. Section analyses of AFM images (right panels in Fig. 1) provide a more detailed insight on the surface morphology. They show that surface A is fairly smooth with typical features of 0.1–1 nm while the morphology of surface B is dominated by 50–100 nm wide features with an average height of 20 nm. It is interesting to note that although surface C is characterized by the largest substrate depth and is composed of 1–3 μm size features (Fig. 1c), these features are very smooth on a local scale of 200 nm used for section analysis. The peak-to-peak variation on this scale is 0.6–1 nm for surface A, 20–40 nm for surface B, and only 3–5 nm for surface C. It follows that despite the significant differences in the roughness of surfaces A and C they are quite similar on the scale that is of interest for ion–surface collisions.

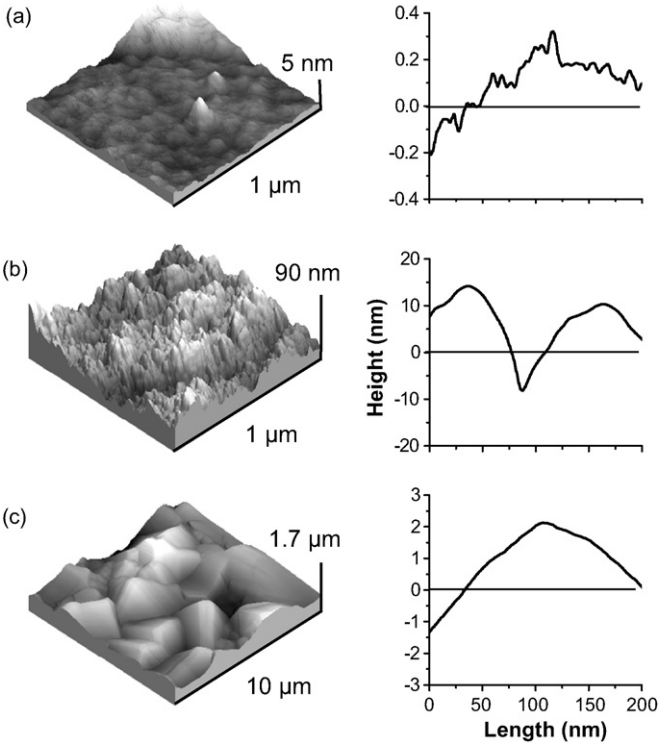

Fig. 1. 3D AFM images (left) and typical section analyses (right) of surfaces (a) A, (b) B, and (c) C. The substrate depth is ~3.2 nm for surface A, ~33 nm for surface B, and ~1.1 μm for surface C.

3.2. SID spectra

Fig. 2a–c shows 51 eV SID spectra of singly protonated des-Arg^1-bradykinin on surfaces A, B, and C, respectively. All spectra contain the major primary fragments of des-Arg^1-bradykinin, M-H_2O and y_6, along with a large number of high-energy fragments including y-ions, b-ions, internal fragments, and immonium ions. Similar fragmentation pattern for this peptide was reported in our previous work [35]. It is interesting to note that fragmentation patterns obtained on the three diamond surfaces are almost identical. In contrast, total scattered signal is affected by surface roughness. Fig. 2 shows that SID signal decreases with increase in surface roughness. Total scattered signal obtained using a smooth surface A is two times higher than the signal obtained using surface B and two to three times higher than the signal obtained using surface C. We attribute this difference to the lower probability of ion neutralization and soft-landing on smooth surfaces. It is likely that rough diamond targets facilitate multiple collisions along the trajectories of scattered ions resulting in a more efficient damping of the kinetic energy of scattered ions followed by trapping and possibly neutralization of the ions on the surface, while the probability for multiple collisions is relatively small for smooth surfaces.

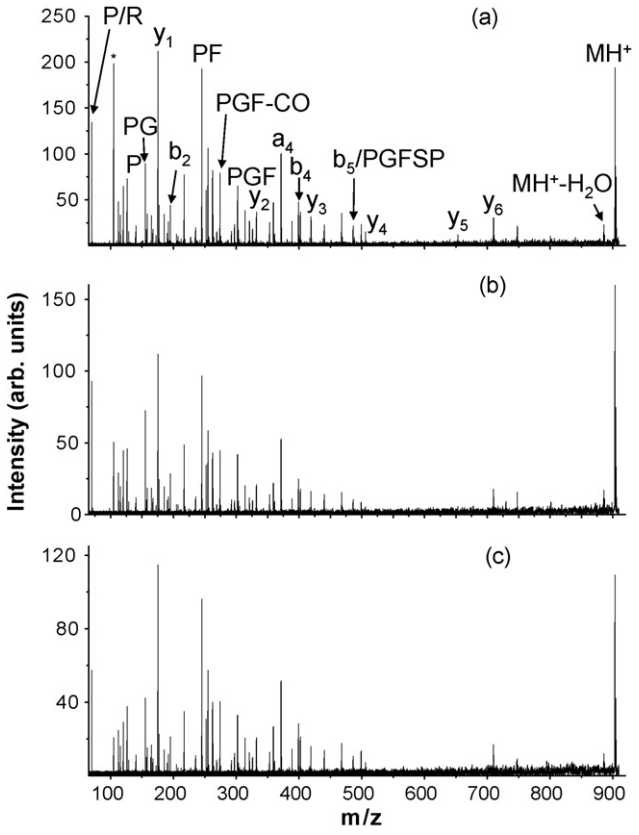

Fig. 2. SID spectra of the protonated des-Arg[1]-bradykinin at 51 eV collision energy on surfaces (a) A, (b) B, and (c) C. The asterisk (*) indicates the noise peaks.

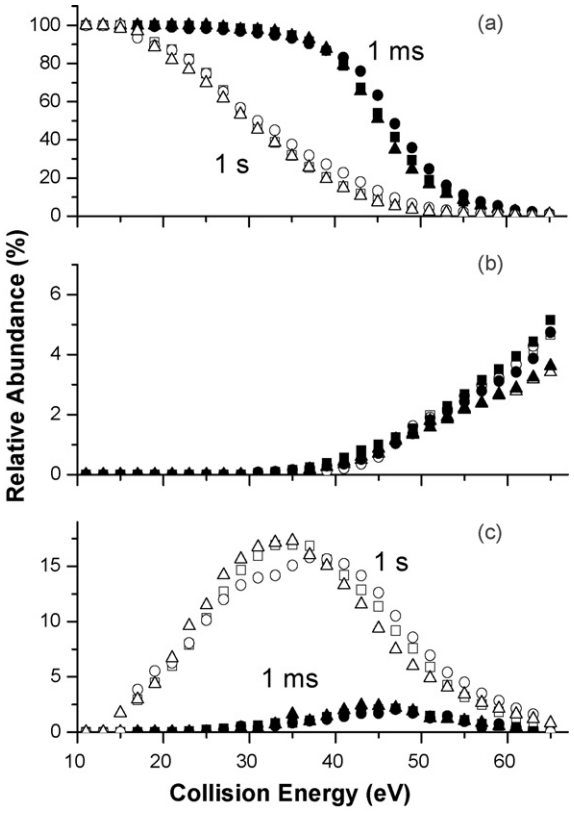

Fig. 3. Time- and energy-resolved fragmentation efficiency curves (TFECs) for: (a) protonated precursor ion, $[M+H]^+$; (b) immonium F ion, and (c) y_6 fragment of the protonated des-Arg[1]-bradykinin for reaction delays 1 ms (filled symbols) and 1 s (open symbols) for surfaces A (■) and (□), B (●) and (◯), and C (▲) and (Δ).

Time- and energy-resolved SID data is a very sensitive tool for investigating the influence of the physical and chemical properties of SID targets on the energy transfer into complex ions [8]. Our previous study demonstrated a sharp transition in fragmentation behavior of des-Arg[1]-bradykinin as a function of collision energy [35]. Low-energy SID spectra are dominated by fragments that are formed via a slow fragmentation process and exhibit a strong time dependence, while many high-energy fragments are formed by instantaneous dissociation of the precursor ion on the surface (shattering). Wide internal energy distribution deposited by collision with a stiff diamond surface provides an efficient mixing between the primary time-dependent (TD) reaction channels and time-independent (TI) pathways. It is important to note that TI fragments are more sensitive to the high-energy tail of the EDF, while the kinetics and energy dependence of TD fragments is largely determined by the low-energy part of the EDF.

Fig. 3 shows comparison of the experimental time- and energy-resolved fragmentation efficiency curves (TFECs) for the precursor ion (MH^+), TD fragment (y_6) and TI fragment (F) of the protonated des-Arg[1]-bradykinin on the three surfaces for reaction time of 1 ms and 1 s. Good overlap between the experimental results from the three surfaces was obtained through multiple repeated experiments, suggesting that the energy transfer efficiency in collisions of peptide ions with surfaces is largely independent of the surface morphology. It follows that EDFs and average T → V energy transfer efficiencies are similar for all of three diamond surfaces.

3.3. Modeling results

RRKM modeling of the experimental data provides quantitative information on the dependence of the internal energy distributions deposited into ions on surface morphology. Fig. 4 shows results of RRKM modeling of the precursor ion SCs obtained on surface A for reaction delays of 1 ms, 50 ms, 100 ms, and 1 s. Similar quality fits (not shown) were obtained for SCs obtained using surfaces B and C.

Average energy transfer efficiencies obtained from the modeling are shown in Table 1. The T → V transfer efficiencies are

Table 1
Results of the RRKM modeling of the precursor ion survival curves[a]

Fitting results	% T → V
Diamond surfaces	
A	19.7 (±0.7)
B	19.0 (±0.7)
C	19.9 (±0.8)

[a] $E_0 = 1.17$ (±0.05) eV is the threshold energy, $\Delta S^{\ddagger} = -22.1$ cal/(mol K) is the activation entropy, T → V transfer (%) is the percentage of the ions' kinetic energy converted to the internal energy upon collision.

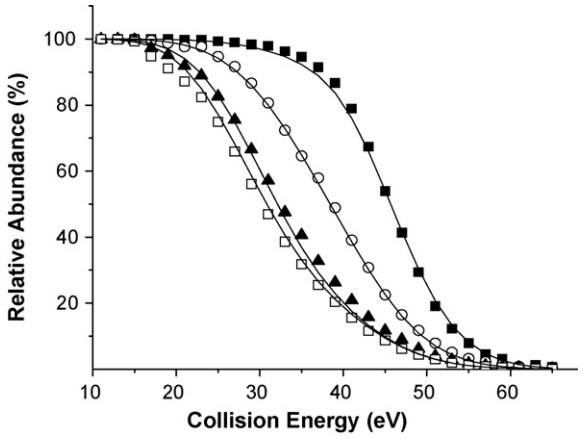

Fig. 4. RRKM modeling fit (lines) of experimental data (symbols) for parent ion survival curves for reaction delays of 1 ms (■), 10 ms (◯), 50 ms (▲), and 1 s (□) on surface A (E_0 = 1.17 eV, $\Delta S^{\ddagger}$ = −22.1 cal/(mol K) [35]).

very similar for the three surfaces. The value obtained using surface B is in a good agreement with the previously reported value for CVD layer on titanium substrate (19.2%) [8] demonstrating excellent reproducibility of the experimental data.

Internal energy distributions deposited into the precursor ion upon collisions with different surfaces at 31 and 51 eV are shown in Fig. 5. Internal energy distributions are Boltzmann-like functions that become wider and shift to higher internal energies with increase in collision energy. Fig. 5 shows an almost perfect overlap between EDFs obtained for surfaces A and C, while slightly broader EDF was obtained for surface B. From our earlier discussion it follows that surfaces A and C are characterized by a very similar local roughness. It is therefore not surprising that identical EDFs are obtained for these two surfaces.

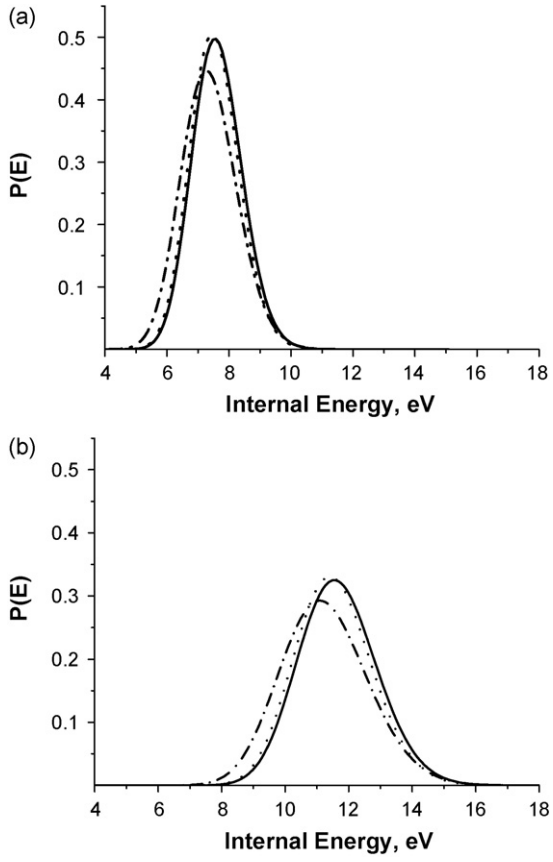

Fig. 5. Comparison of internal energy distributions following collisions of protonated des-Arg^1-bradykinin with three diamond surfaces: A (solid line), B (dash-dot line), and C (dotted line) at collision energies of (a) 31 eV and (b) 51 eV.

Substantially larger local roughness of the surface B is reflected in somewhat broader EDF and a slightly lower average energy transfer obtained for this surface. This broadening can be rationalized as follows. Although in our experiments ions are directed toward the surface along the surface normal, the incidence angle of individual collisions is determined by the surface morphology. Collisions with rough surfaces efficiently sample a broader range of incidence angles than collisions with smooth surfaces. Classical trajectory calculations demonstrated that the energy transfer efficiency increases with decrease in the incidence angle and reaches its maximum for normal-incidence collisions. For example, calculations predict that for collisions of protonated diglycine with a diamond surface the T → V transfer efficiency decreases from 20% for normal-incidence collision to 15% for 45° collision [34]. It follows that normal-incidence collisions with smooth surfaces result in higher T → V transfer efficiency than collisions with rough surfaces. In addition, effective averaging over different incidence angles in collisions with rough surfaces results in broadening of the EDF.

Our results provide first experimental evidence that local roughness of SID targets has only a minor effect on the energy transfer efficiency in collisions of large ions with surfaces. However, it is reasonable to assume that because the morphology of the surface affects the incidence angle on the local scale of collision, surface roughness may confound experimental studies of the effect of the incidence angle on the energy transfer in collisions. For example, beam experiments on the scattering of ethanol ions from oil coated carbon and stainless steel surfaces, concluded that the efficiency of energy transfer was independent on the angle of incidence [41,42], which contradicts classical trajectory calculations. Hase and co-workers later suggested that this discrepancy could be attributed to the differences in the roughness of surfaces used in experiments and in calculations [10]. Our study supports this conclusion.

4. Summary

Time- and energy-resolved SID of singly protonated octapeptide des-Arg^1-bradykinin (PPGFSPFR) was used to study the effect of the morphology of the SID target on the T → V transfer efficiency. Three SID diamond targets of varying degree of roughness were quantitatively characterized by AFM in this work. An RRKM-based modeling approach was utilized to extract internal energy distributions deposited into the precursor ion upon collisions with different surfaces and the efficiency of T → V energy transfer. The percent of T → V transfer is very similar for the three surfaces (19.0–19.9%). Furthermore, the width of the energy deposition function (EDF) is only slightly affected by the roughness of the SID target. However, the total signal of scattered ions is affected by the surface morphology.

Specifically, the scattered signal increases with decrease in the surface roughness suggesting that polished diamond surface is a better SID target for practical applications. The results demonstrate that the morphology of a diamond surface has only a minor effect on the energy transfer in ion–surface collisions and a strong effect on the recoil efficiency.

Acknowledgments

The research described in this manuscript was performed at the W.R. Wiley Environmental Molecular Sciences Laboratory (EMSL), a national scientific user facility sponsored by the U.S. Department of Energy's Office of Biological and Environmental Research and located at Pacific Northwest National Laboratory (PNNL). PNNL is operated by Battelle for the U.S. Department of Energy. Research at EMSL was supported by the grant from the Separations and Analysis Program within the Chemical Sciences Division, Office of Basic Energy Sciences of the US Department of Energy.

References

[1] A.R. Dongré, Á. Somogyi, V.H. Wysocki, J. Mass Spectrom. 31 (1996) 339.
[2] V. Grill, J. Shen, C. Evans, R.G. Cooks, Rev. Sci. Instrum. 72 (2001) 3149.
[3] J. Laskin, J.H. Futrell, Mass Spectrom. Rev. 22 (2003) 158.
[4] O. Meroueh, W.L. Hase, J. Am. Chem. Soc. 124 (2002) 1524.
[5] K. Song, O. Meroueh, W.J. Hase, Chem. Phys. 118 (2003) 2893.
[6] J. Laskin, J.H. Futrell, J. Chem. Phys. 116 (2002) 4302.
[7] T.H. Bailey, J. Laskin, J.H. Futrell, Int. J. Mass Spectrom. 222 (2003) 313.
[8] J. Laskin, J.H. Futrell, J. Chem. Phys. 119 (2003) 3413.
[9] Y.F. Wang, W.L. Hase, J. Am. Soc. Mass Spectrom. 14 (2003) 1402.
[10] J.P. Wang, S.O. Meroueh, Y.F. Wang, W.L. Hase, Int. J. Mass Spectrom. 230 (2003) 57.
[11] J. Laskin, J.H. Futrell, J. Am. Soc. Mass Spectrom. 14 (2003) 1340.
[12] R.G. Cooks, T. Ast, T. Pradeep, V. Wysocki, Acc. Chem. Res. 27 (1994) 316.
[13] F.M. Fernández, L.L. Smith, K. Kuppannan, X. Yang, V.H. Wysocki, J. Am. Mass Spectrom. 14 (2003) 1387.
[14] C. Gu, V.H. Wysocki, A. Harada, H. Takaya, I. Kumadaki, J. Am. Chem. Soc. 121 (1999) 10554.
[15] T. Pradeep, S.A. Miller, R.G. Cooks, J. Am. Soc. Mass Spectrom. 4 (1993) 769.
[16] W.R. Koppers, J.H.M. Beijersbergen, T.L. Weeding, P.G. Kistemaker, A.W. Kleyn, J. Chem. Phys. 107 (1997) 10736.
[17] Md.A. Mabud, M.J. DeKrey, R.G. Cooks, Int. J. Mass Spectrom. Ion Process. 67 (1985) 285.
[18] M.J. DeKrey, Md.A. Mabud, J.E.P. Syka, R.G. Cooks, Int. J. Mass Spectrom. Ion Process. 67 (1985) 295.
[19] M.E. Bier, J.W. Amy, R.G. Cooks, J.E.P. Syka, P. Ceja, G. Stafford, Int. J. Mass Spectrom. Ion Process. 77 (1987) 31.
[20] B.E. Winger, P.K. Julian, R.G. Cooks, C.E.D. Chidsey, J. Am. Chem. Soc. 113 (1991) 8967.
[21] T. Tepnual, L. Feketeova, V. Grill, P. Scheier, Z. Herman, T.D. Mark, Int. J. Mass Spectrom. 244 (2005) 164.
[22] K. Vekey, A. Somogyi, V.H. Wysocki, J. Mass Spectrom. 30 (1995) 212.
[23] M.R. Morris, D.E. Riederer, B.E. Winger, R.G. Cooks, T. Ast, C.E.D. Chidsey, Int. J. Mass Spectrom. Ion Process. 122 (1992) 181.
[24] S.B. Wainhaus, H.J. Lim, D.G. Schultz, L. Hanley, J. Chem. Phys. 106 (1997) 10329.
[25] R.D. Beck, J. Rockenberger, P. Weis, M.M. Kappes, J. Chem. Phys. 104 (1996) 3638.
[26] M.E. Saecker, S.T. Govoni, D.V. Kowalski, M.E. King, G.M. Nathanson, Science 252 (1991) 1421.
[27] S.R. Cohen, R. Naaman, J. Sagiv, Phys. Rev. Lett. 58 (1987) 1208.
[28] J.A. Burroughs, S.B. Wainhaus, L. Hanley, J. Phys. Chem. 98 (1994) 10913.
[29] H.L. de Clercq, A.D. Sen, A.K. Shukla, J.H. Futrell, Int. J. Mass Spectrom. 212 (2001) 491.
[30] J. Laskin, E. Denisov, J.H. Futrell, J. Phys. Chem. B 105 (2001) 1895.
[31] J. Laskin, C. Lifshitz, Principle of Mass Spectrometry Applied to Biomolecules, Wiely, New York, 2006.
[32] J. Laskin, J.H. Futrell, Mass Spectrom. Rev. 24 (2005) 135.
[33] F.M. Fernandez, V.H. Wysocki, J.H. Futrell, J. Laskin, J. Am. Soc. Mass Spectrom. 17 (2006) 700.
[34] A. Rahaman, J.B. Zhou, W.L. Hase, Int. J. Mass Spectrom. 249 (2006) 321.
[35] J. Laskin, T.H. Bailey, J.H. Futrell, J. Am. Chem. Soc. 125 (2003) 1625.
[36] J. Laskin, E.V. Denisov, A.K. Shukla, S.E. Barlow, J.H. Futrell, Anal. Chem. 74 (2002) 3255.
[37] S.A. Shaffer, K. Tang, G.A. Anderson, H.R. Udseth, R.D. Smith, Rapid Commun. Mass Spectrom. 10 (1997) 1813.
[38] M.W. Senko, J.D. Canterbury, S. Guan, A.G. Marshall, Rapid Commun. Mass Spectrom. 10 (1996) 1839.
[39] J. Laskin, M. Byrd, J. Futrell, Int. J. Mass Spectrom. 195 (2000) 285.
[40] J. Laskin, J.H. Futrell, J. Phys. Chem. A 104 (2000) 5484.
[41] R. Worgotter, J. Kubista, J. Zabka, Z. Dolejsek, T.D. Mark, Z. Herman, Int. J. Mass Spectrom. 174 (1998) 53.
[42] J. Kubista, Z. Dolejsek, Z. Herman, Eur. Mass Spectrom. 4 (1998) 311.